Geological Society of America Bulletin, published online on 2 October 2012 as doi:10.1130/B30324.1

Geological Society of America Bulletin

Gobi-Tianshan connections: Field observations and isotopes from an early Permian arc complex in southern Mongolia

R.C. Economos, S.R. Paterson, L.O. Said, M.N. Ducea, J.L. Anderson and A.J. Padilla

Geological Society of America Bulletin published online 2 October 2012;
doi: 10.1130/B30324.1

Notes

Geological Society of America Bulletin, published online on 2 October 2012 as doi:10.1130/B30324.1

Gobi-Tianshan connections: Field observations and isotopes from an early Permian arc complex in southern Mongolia

R.C. Economos[1,†,§], S.R. Paterson[1], L.O. Said[2], M.N. Ducea[3,4], J.L. Anderson[1], and A.J. Padilla[5]
[1]*Department of Earth Sciences, University of Southern California, Los Angeles, California 90089, USA*
[2]*Department of Geology, School of Geology and Petroleum Engineering, Mongolian University of Science and Technology, Ulaanbaatar 210646, Mongolia*
[3]*Department of Geosciences, University of Arizona, Tucson, Arizona 85721, USA*
[4]*Universitatea Bucuresti, Facultatea de Geologie si Geofizica, Bucuresti 010041, Romania*
[5]*Department of Earth and Environmental Science, Vanderbilt University, Nashville, Tennessee 37240, USA*

ABSTRACT

The Tianshan orogen, in the southern Central Asian orogenic belt, consists of continental fragments stitched together during mid- to late Paleozoic arc magmatism generated by the closure of the paleo–Asian Ocean. Controversy persists regarding the timing of final structural amalgamation of the region and therefore whether Permian magmatism was generated in a subduction or intraplate environment. Based on new field mapping, zircon U-Pb geochronology, and isotope data from the 295–290 Ma Gobi-Tianshan intrusive complex in southwestern Mongolia, we argue that this complex is a voluminous intermediate batholith generated by subduction and that it is related to plutons of similar age and character in Tianshan tectono-magmatic belts to the west. In the study area, as well as in Carboniferous and Permian plutons across the Tianshan, mantle isotopic signatures remain consistently primitive. Permian plutons show an increase in radiogenic Sr with no concurrent decrease in radiogenic Nd, which may be due to the influence of subducting continental sediment in the early Permian. This model explains the transitional nature of magmatic compositions and structures in the Gobi-Tianshan intrusive complex.

INTRODUCTION

The Central Asian orogenic belt is a tectonic collage of magmatic arcs and intervening basins constructed mainly during the Neoproterozoic to Paleozoic (for reviews, see Fillipova et al., 1990; Şengör and Natal'in, 1996; Badarch et al., 2002). The southernmost portion of this belt, today stretching from Kazakhstan to northeastern China, preserves a record of the late Paleozoic closure of the paleo–Asian Ocean by subduction and ultimate docking of the Tarim continental block with the resulting accreted terranes (Coleman, 1989; Dobretsov et al., 1995). The Tianshan section of the orogenic belt (Fig. 1) is located predominantly in the Xinjiang region of northwestern China, and its topographic expression is due to modern uplift related to Himalayan transpressional tectonics (Molnar and Tapponnier, 1975). The structural character of the Tianshan is one of lenticular (E-W elongate) blocks separated by long, regional-scale faults that complexly interleave mid- and late Paleozoic magmatic and accretionary units (e.g., fig. 4 *in* Xiao et al., 2009). Due to the motion of these strike-slip faults, related blocks may be telescoped across hundreds of kilometers, reminiscent of systems found in northwestern Canada and southern Alaska (e.g., Plafker et al., 1989).

Extensive mapping, structural, geochemical, and geochronological work in this area has reached a critical stage, and several large-scale tectonic syntheses have recently been published (Charvet et al., 2007; Kröner et al., 2007; Gao et al., 2009; Xia et al., 2004, 2008; Xiao et al., 2008, 2009, 2010; Wang et al., 2009). These share some conclusions, including the ages of major magmatic events and the location of large-scale faults. However, significant disagreement remains as to the location, facing, and timing of closure structures. Differences in interpretation largely stem from difficulties in correlating and contrasting accretionary components and sedimentary successions of the Tianshan due to significant disruption by post-Paleozoic fault movement. Relating arc plutons to accretionary packages in the Tianshan nearly always requires correlation across one or more major subsequent strike-slip structures with no constraints on amounts of offset such as piercing points. Furthermore, the geochronology of blueschist and accretionary units has proven to be complex; estimates of latest subduction range from Devonian to Triassic (Zhang et al., 2007; Xiao et al., 2009; Wang et al., 2010; Su et al., 2010). In this study we have addressed this problem by using geochronology and geochemistry to relate magmatic fragments to each other and to source materials implied by geochemical constraints.

It is clear from structural and magmatic changes across the Tianshan that the Carboniferous to Permian was a time of dramatic transition. Magmatism in the Tianshan and southern Mongolia transitioned from generally calc-alkaline to alkaline or even S-type (e.g., Seltmann et al., 2010). This period was concurrent with a change from a compressional regime to a translational regime that generated strike-slip faults hundreds of kilometers long (de Jong et al., 2009). However, the relative timing of these magmatic and structural events is poorly constrained, due in part to the paucity of high-precision geochronology across a complex area.

In this paper, we assess two contrasting models that have been proposed to describe the cessation of subduction in the Tianshan: one based on amalgamation in Carboniferous times, and the other during the mid-Permian. In the first model, magmatism is thought to have been generated by subduction that continued through the early Permian across the Tianshan (Briggs et al., 2007; Zhang et al., 2007; Xiao et al., 2009), immediately followed by docking of the Tarim continental block with accreted Tianshan arcs and regionwide strike-slip faulting. In the second, structural consolidation is thought to have occurred during mid-Carboniferous times,

†E-mail: economos@ucla.edu
§Current address: Department of Earth and Space Sciences, University of California, Los Angeles, California 90095, USA

Geological Society of America Bulletin, published online on 2 October 2012 as doi:10.1130/B30324.1

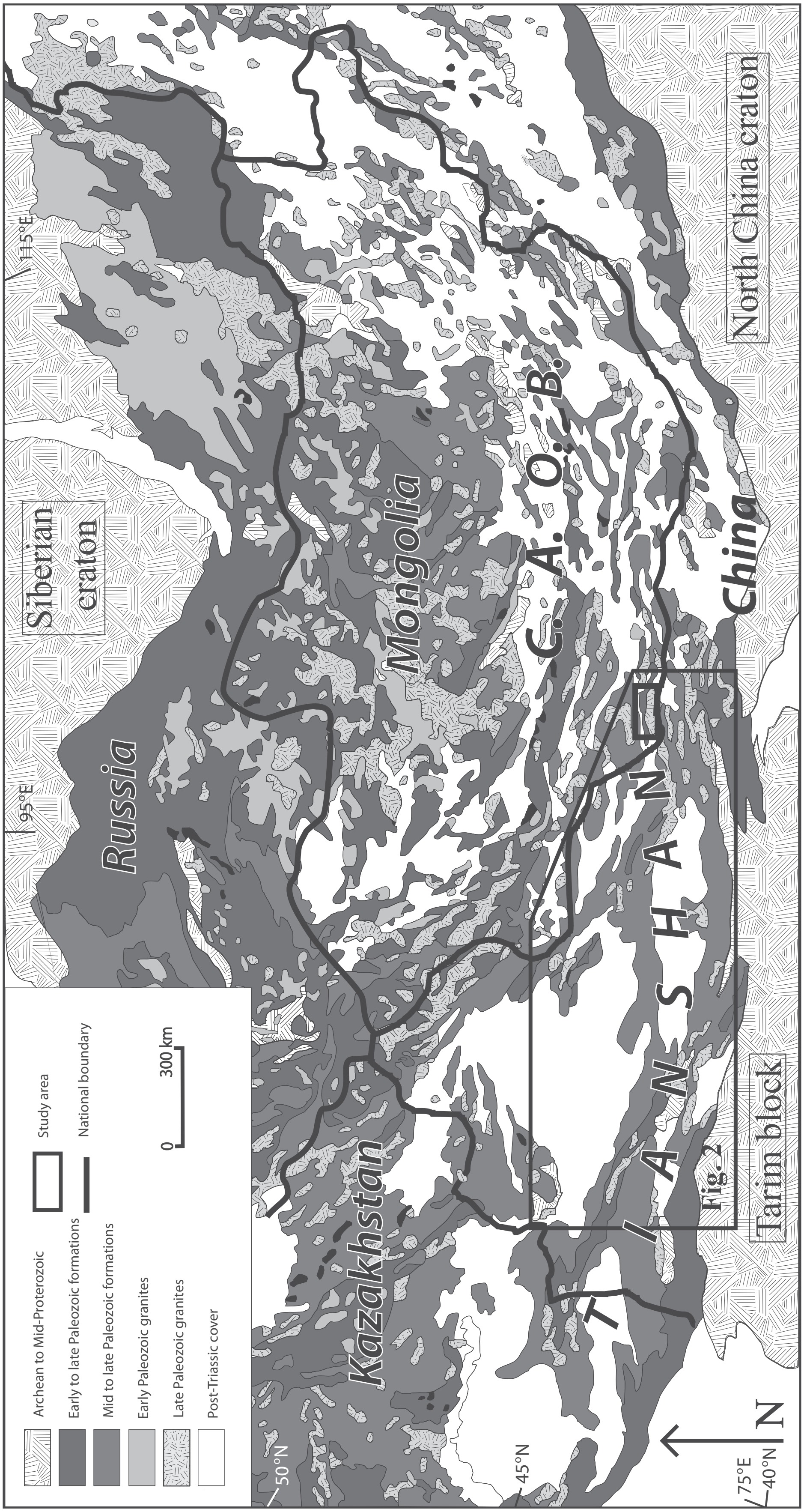

Figure 1. Map of the Central Asian orogenic belt (C.A.O.B.) and Tianshan (modified after Jahn et al., 2000b).

and was followed by a transtensional regime in which magmas of Permian age were generated (Wang et al., 2009). Arc characteristics of this magmatism were interpreted to result from involvement of arc-modified lower crust and mantle in a postcollisional, possibly hotspot-influenced environment (Xia et al., 2004; Han et al., 2010; Tang et al., 2010). A variation on this model makes a similar prediction for the formation of Permian magmatic bodies, but argues that both Carboniferous magmatism and Permian magmatism are postcollisional and related to rifting (Gu et al., 2000; Xia et al., 2004, 2008; Li et al., 2010).

The study area, the Gobi-Tianshan intrusive complex, is a 3400 km^2 Permian batholith at the eastern end of the Tianshan where the belt crosses the border between China and Mongolia. We investigate the relationship between the Gobi-Tianshan intrusive complex and other Tianshan magmatic belts by comparing the Gobi-Tianshan intrusive complex to published structural data, geochronology, and geochemistry from the Tianshan and East Junggar regions. We use insights gleaned from the intrusive complex to guide an interpretation of regional isotopic signals observed in magmatic rocks from across the Tianshan. This interpretation is then fit into the broader sedimentological, structural, and tectonic picture of the Tianshan at this time. This approach highlights compositional, and in particular isotopic, signals from across the Tianshan that must be explained by any comprehensive magmatic model.

These issues bear on the types and proportions of source material contributions in a system that is purported to yield the most volumetrically significant generation of juvenile crustal material in Paleozoic time (Jahn et al., 2000a). The distinct isotopic character (from depleted mantle, Archean continental crust, and mobile belts) presents the opportunity to constrain the variation in magma source contribution during an evolving continental collision. Finally, improved constraints on the timing of collisional events in the Tianshan will contribute to a more complete view of the process of structural consolidation that occurred across thousands of kilometers now preserved in northern China and southern Mongolia.

GEOLOGIC SETTING

Regional Geology

Late Paleozoic igneous rocks of the Tianshan were intruded into a very diverse crust that included Proterozoic continental blocks and Ordovician to Devonian arc complexes and their associated basins (Charvet et al., 2007; Kröner et al., 2010) (Fig. 2). In the Carboniferous, voluminous magmatism, mainly intermediate in composition, is generally interpreted to have been generated in an arc setting (Xia et al., 2004; Gu et al., 2005; Q. Wang, et al., 2007; Zheng et al., 2007). The Permian was a time of tectonic and magmatic transition. Permian plutons shift from hydrated granodiorite compositions to high-K granite, alkaline, and S-type compositions (Chen et al., 2000; Chen and Jahn, 2004; Gu et al., 2005; B. Wang, et al., 2007, 2009). Swarms of mafic to intermediate dikes were emplaced coeval with or shortly after Permian magmatism in several regions of the Tianshan (Allen et al., 1991; Gu et al., 2005; Shu et al., 2011; Carroll et al., 1995). These dike swarms were contemporaneous with, or postdated by, an orogenwide anastamosing strike-slip fault system that affected the entire Tianshan, indicating a first-order shift from compressional to translational tectonic regime (Laurent-Charvet et al., 2003; de Jong et al., 2009). This faulting was coincident with the cessation of significant magmatism in the Tianshan, except minor alkaline plutons (e.g., Zhang et al., 2008).

The geology of southwestern Mongolia shares these first-order geological characteristics. The study area, the Gobi-Tianshan intrusive complex (also called Zamyn Belgekh pluton by Hanzl et al., 2008a), is a Permian igneous complex located in the southwestern corner of Mongolia, along strike to the east of Tianshan tectono-magmatic belts (Fig. 2). Initial mapping (Hanzl et al., 2008b) revealed a large, E-W–trending dioritic to granitic batholith and adjacent volcanic rocks (Fig. 3). The northern margin of this batholith is in fault contact with complex accretionary and volcano-sedimentary metamorphic packages of likely Devonian age (Geomin, 2003; Hanzl et al., 2008b). All of these units are bounded to the north by the active Gobi-Tianshan fault zone, one of the largest active strike-slip systems in the world (Cunningham et al., 1996).

Fundamental regional correlations must be addressed in order to understand the implications of the findings from the Gobi-Tianshan intrusive complex for the broader Tianshan system. Immediately to the west of the Gobi-Tianshan intrusive complex, there is the Kelameili-Harlik belt (Charvet et al., 2007). It is composed of widely distributed calc-alkaline to alkaline plutons and mafic dikes ranging from mid-Carboniferous to early Permian in age (Gu et al., 2005; Wang et al., 2010; Yuan et al., 2010). The Kelameili fault zone is a major Paleozoic structure, associated with adjacent mafic/ultramafic complexes, that bounds the Harlik range to the north and may be contiguous with faults to the north of the Gobi-Tianshan intrusive complex.

Two mountain ranges trend away from the Harlik belt, one to the NW (the East Junggar region) and the Bogda Mountains to the SW, divided by the Junggar Basin (Fig. 2). The Gobi-Tianshan intrusive complex and the Harlik region may be related to one or both of these ranges. Though geochronology is scarce, some confirmed Carboniferous to Permian magmatic dikes and other igneous bodies were emplaced in the Bogda region to the west of the Gobi-Tianshan intrusive complex and Harlik range (Fig. 2) (Allen et al., 1991; Xia et al., 2004, 2008; Shu et al., 2011). Some workers consider the Bogda region to represent a Carboniferous arc complex, along with likely associated materials from the region south of the Tu Ha Basin, where regionally foliated metamorphic rocks host a chain of lenticular intrusive bodies (e.g., Bogda arc sensu Charvet et al., 2007) (Fig. 2).

Plutons of the East Junggar region are early Permian (294–284 Ma), transitional from calc-alkaline to alkaline, and in some places display arc-geochemical characteristics (Chen and Jahn, 2004; Wang et al., 2010). While ε_{Nd} is positive, initial $^{87}Sr/^{86}Sr$ isotopic ratios vary over a wide range, including values up to 0.7115 (Han et al., 1997). The Junggar Basin itself is underlain primarily by volcanic and subordinate sedimentary sequences. Volcanic rocks are Early Devonian and Carboniferous; those of Carboniferous age are also of arc geochemical affinity and yield positive ε_{Nd} and low $^{87}Sr/^{86}Sr_{(t)}$ values (Zheng et al., 2007).

Although the present geographic position of the western Tianshan is somewhat distant from the Gobi-Tianshan intrusive complex, Paleozoic plutons there share similar chronological, petrological, and geochemical characteristics, perhaps indicating a related magmatic history. The Yili block, southwest of the Junggar Basin, is cored by Proterozoic continental crust and hosts Carboniferous and Permian 307–289 Ma igneous rocks (Chen et al., 2000; Q. Wang et al., 2007; Wang et al., 2008) (Fig. 2). These bodies throughout the block carry arc-geochemical signatures, suggesting an active arc on the Yili margin in Carboniferous times (Q. Wang, et al., 2007). Permian-age magmatic bodies show transitional chemistry from I-type to S-type (Chen et al., 2000) and also include high-K calc-alkaline granites (Q. Wang et al., 2007). Yili block magmas yield the only slightly negative ε_{Nd} values in the region, likely owing to contamination by ancient continental crust (Xia et al., 2008). Initial Sr isotope ratios again range to high values, similar to ratio ranges found in the East Junggar. The Yili block is fault bounded to the north against the Northern Tianshan mélange complex (Wang et al., 2009; Xiao et al., 2009) (Fig. 2). To the south, it is fault bounded against

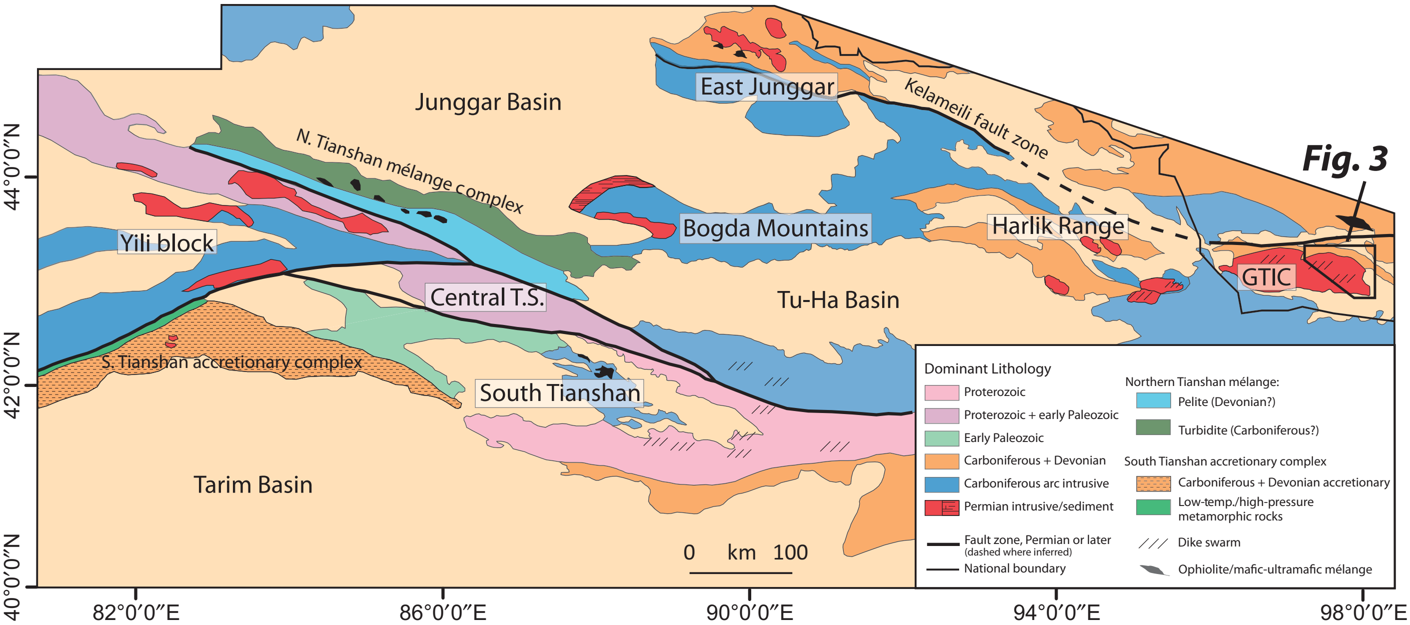

Figure 2. Synthesis map of the Tianshan and southwest Mongolia region, showing the extent of Carboniferous and confirmed early Permian magmatism (after: Gu et al., 2000, 2005; Badarch et al., 2002; Chen and Jahn, 2004; Charvet et al., 2007; Long et al., 2008; Hanzl et al., 2008b; Wang et al., 2009; C.S. Wang et al., 2010; Xiao et al., 2009; Li et al., 2010; Yuan et al., 2010). GTIC—Gobi-Tianshan intrusive complex.

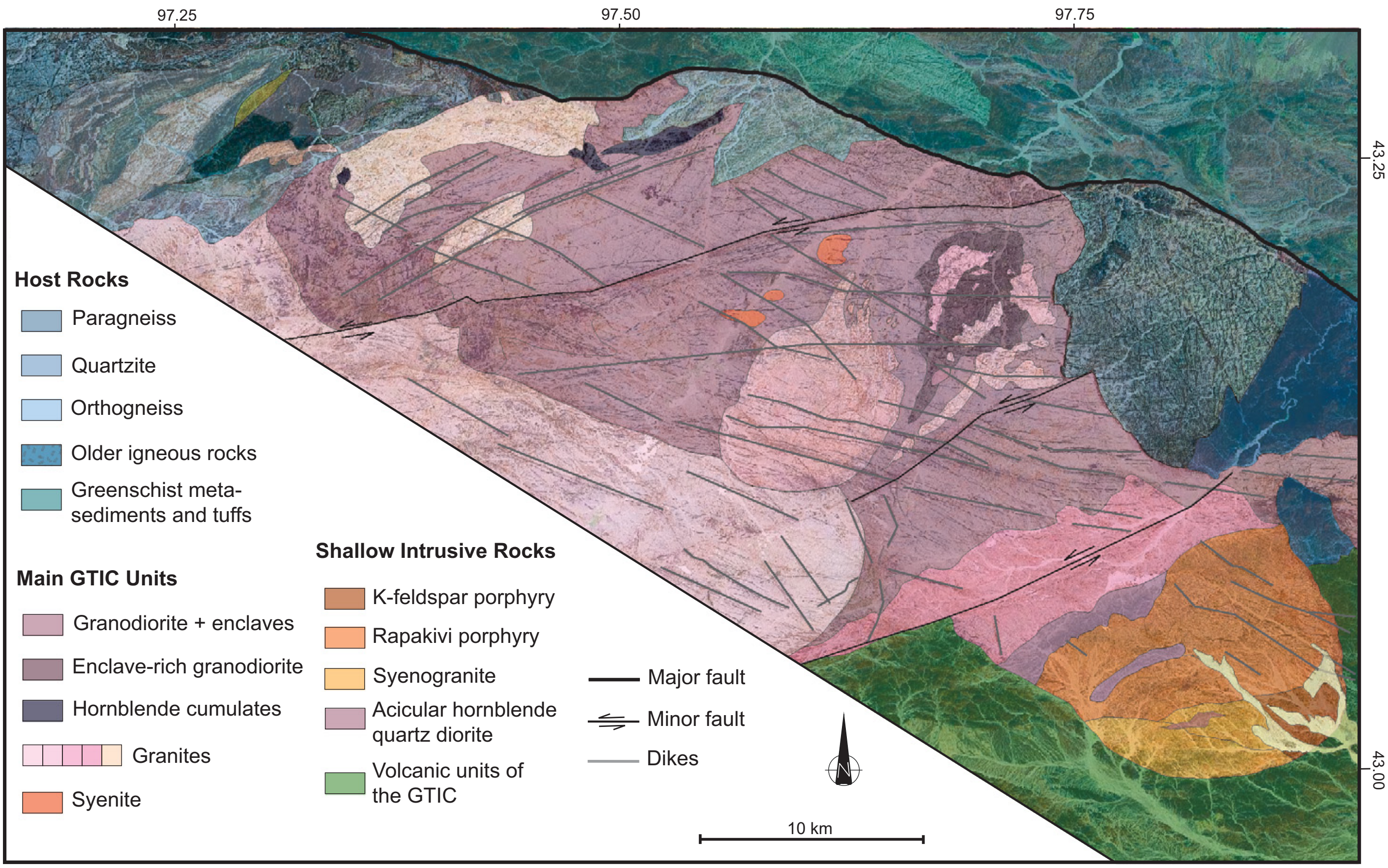

Figure 3. Reconnaissance-scale map of the Gobi-Tianshan intrusive complex (GTIC).

the Southern Tianshan–Central Tianshan region, which is composed primarily of Proterozoic basement intruded by a complex series of mid- to late Paleozoic magmatic rocks. This block is truncated to the south against a package of high-pressure, low-temperature schists, mafic complexes, and accretionary rocks. These units are evidence for a zone of former subduction and subsequent suturing (Gao et al., 1995; Xiao et al., 2004). Finally, the southernmost region of the Tianshan, the Tarim block, consists of an Archean to Proterozoic core upon which an early to mid-Paleozoic passive margin developed (Hu et al., 1998). This margin may have been disrupted by late Paleozoic magmatism (Xiao et al., 2004). Mafic dikes penetrated the lower Permian sedimentary section in the western Tarim region before a diachronous regressive transition to subaerial sedimentation in the lower and upper Permian (Carroll et al., 1995).

Geology of the Gobi-Tianshan Intrusive Complex

The Gobi-Tianshan intrusive complex is largely composed of late Paleozoic igneous rocks, with only minor schist host-rock screens and rafts, mostly located in the northernmost exposures. Immediately to the north of the Gobi-Tianshan intrusive complex, there is a wedge of metasedimentary rocks that includes impure sandstones, schists, minor marbles, and rare pillow basalts. This package was deformed and subsequently intruded by plutons of unknown age (Figs. 3 and 4A). Rafts of similar metasedimentary material are found in the Gobi-Tianshan intrusive complex. A second metamorphic package is juxtaposed against the complex along a large-scale fault with shallowly plunging slickenlines. These metamorphic rocks are greenschist-grade metavolcanic and volcaniclastic rocks that are interlayered with minor marble (Geomin, 2003).

Voluminous enclave-bearing granodioritic intrusions dominate the central portions of the complex. These plutons have a typical hydrated assemblage of quartz, plagioclase, hornblende, biotite, K-feldspar, sphene, and minor accessory

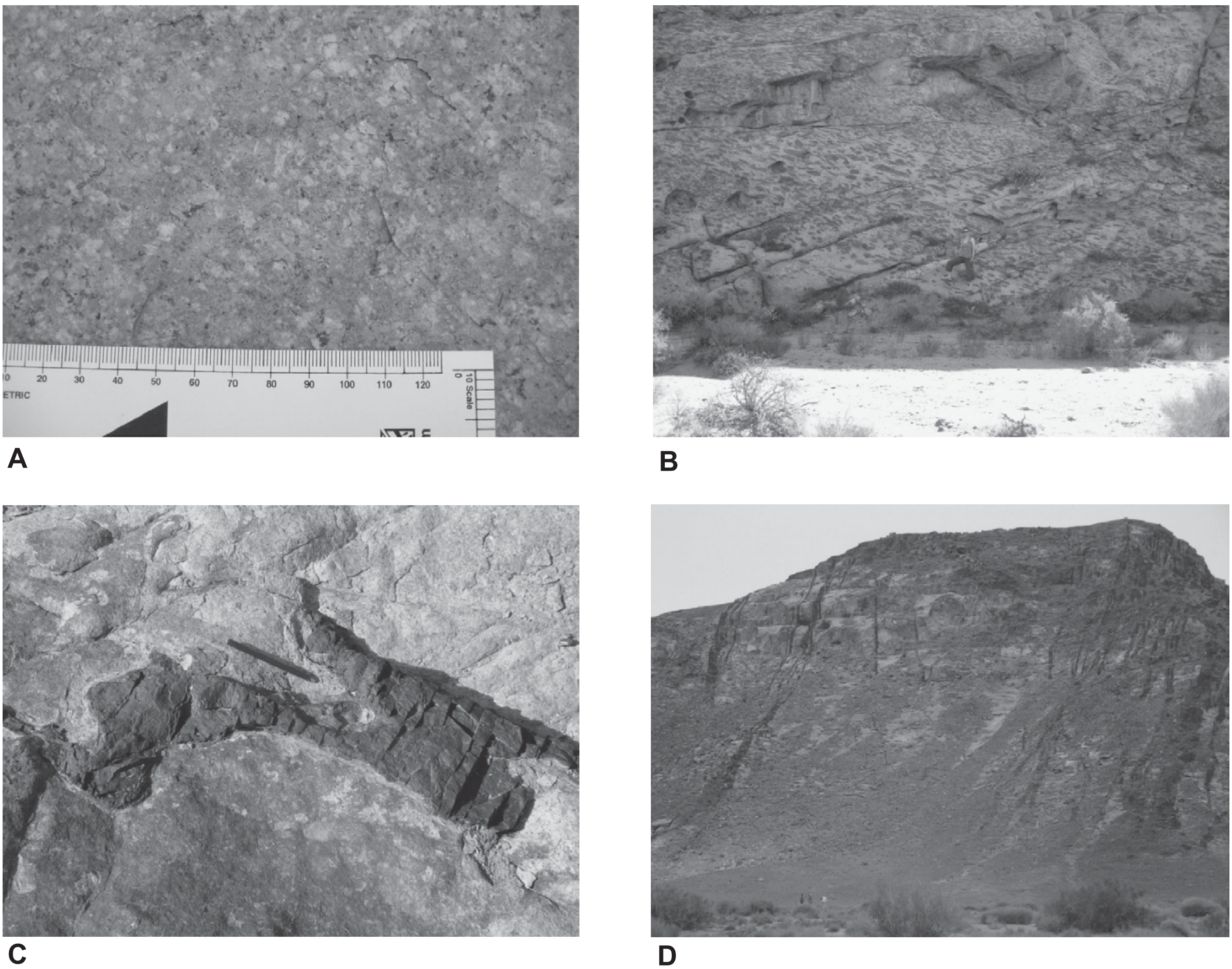

Figure 4. Field photographs from the Gobi-Tianshan intrusive complex: (A) rapakivi porphyry displaying subvolcanic textures and acicular hornblendes; (B) voluminous mafic microgranitoid enclaves in granodiorite (person for scale); (C) intermediate to mafic dikes crosscutting granodiorite (5 inch magnet for scale); and (D) mafic dike that intruded partially molten granodiorite (people in lower left for scale).

phases. Mafic enclaves range from gabbroic to granodioritic composition (Fig. 4B). Their textures range from quenched to gradational with their host granodiorites. Granodiorites of this style represent >50% of magmatism in the Gobi-Tianshan intrusive complex. Magmatic contacts, enclave long-axis orientations, and magmatic fabrics all dip steeply. Granite intrusion was contemporaneous with or slightly postdated granodiorite plutonism, commonly displaying mutually intrusive contacts. In the northern portion of the Gobi-Tianshan intrusive complex, complex interactions among diorite, granite, and mafic dikes are observed, magmatic fabrics become more intense, and this region is generally interpreted as the deepest exposure in the area.

These granodiorite and granite bodies are crosscut by large, shallowly dipping granite sheets with variable textures and mineralogies. Granite sheets vary both in K-feldspar content and mafic mineralogy, although all are high in SiO_2 and include small intrusions of syenogranite. Plutons in the southernmost portions of the Gobi-Tianshan intrusive complex have acicular hornblendes, vugs, porphyritic textures, and intrude volcanic units in the south (Fig. 4D), all implying a subvolcanic environment. They commonly preserve rapakivi feldspars and both biotite and hornblende, suggesting magma temperature shifted and H_2O contents fell during the waning stages of magmatism (Fig. 4A). Based on the structural relationships from north to south, including a sheeted complex, large intermediate plutons, subvolcanic plutons, and a volcanic pile, the Gobi-Tianshan intrusive complex is interpreted as a depth-transect through a magmatic system, an interpretation corroborated by thermobarometry (Padilla et al., 2008; Economos, 2009).

All of these intrusions are crosscut by a dike swarm (Fig. 4C) with a wide compositional range (Hanzl et al., 2008a). Mutually intrusive field relationships indicate that the dikes interacted with still-partially-molten magmas in the central Gobi-Tianshan intrusive complex (Fig. 4D), and clearly stalled and mingled with the exposed subvolcanic granitic units (Fig. 3), interpreted as the latest crystallizing intrusive units presently exposed. Finally, all units, including late dikes, are bounded to the north by large-scale faults.

U-Pb GEOCHRONOLOGY

U-Pb geochronology from the Gobi-Tianshan intrusive complex includes three laser ablation–inductively coupled plasma–mass spectrometry (LA-ICP-MS) ages from the main body (Hanzl et al., 2008a). Weighted average $^{206}Pb/^{238}U$ ages range from 309 to 288 Ma. Kroner et al. (2010) dated a granodiorite from the complex by sensitive high-resolution ion microprobe (SHRIMP) II at ca. 300 Ma, and an orthogneiss xenolith that yielded a range of concordant ages from Neoproterozoic to early Carboniferous, with a main population also at ca. 300 Ma.

In this study, four samples were selected for zircon U-Pb geochronology to constrain the magmatic chronology implied by crosscutting relationships. These include a granodiorite from the main intrusive body (sample number 1407), a syenogranite sheet (15407), an andesite dike (12207), and a rhyolite (5406). The volcanic sample was analyzed to corroborate field evidence of contiguity of plutons with a coeval volcanic section.

Zircon U-Pb geochronology was conducted on a Cameca 1270 secondary ionization mass spectrometer at the University of California, Los Angeles (UCLA), using procedures outlined in Schmitt et al. (2003). Grains were surveyed before analysis using electron backscatter imaging and cathodoluminescence imaging on a Leo 1430VP scanning electron microscope at UCLA. Samples were gold-coated and probed with a mass-filtered, 10–20 nA ^{16}O beam focused to a 30–35-µm-diameter spot. The relative sensitivities for Pb and U were determined on reference zircon AS-3 (Paces and Miller, 1993). Several grains from each sample displayed metamict textures due to expansion of U-rich cores. Fractures in grains were specifically avoided, and data do not indicate significant effects of Pb loss (Table 1).

Data were collected during two separate sessions; run 1 yielded a lower slope than ideal linear calibration curves of UO/U versus Pb/U in zircon standard AS3. Only two samples yielded identical ages within 1σ error utilizing the measured slope of ~0.3 and a forced fit of a more ideal value of 0.5 (5406 and 15407) and are cited here using the measured calibration slope and associated errors. The other two samples were re-run on the same instrument at a later date with improved calibration (1407 and 12207).

Weighted mean $^{206}Pb/^{238}U$ ages (Fig. 5; Table 1) include: the main-body granodiorite (sample 1407) 293 ± 7 Ma, the syenogranitic sheet (sample 15407) 292 ± 13 Ma, and the andesite dike from the dike swarm (sample 12207) 295 ± 5 Ma (a Silurian concordant zircon, interpreted as inherited, and a strongly discordant grain were removed from the average). The rhyolite (sample 5406) yielded an age of 290 ± 12 Ma.

The ages indicate that the Gobi-Tianshan intrusive complex was intruded in earliest Permian time, and the ages overlap or are slightly younger than another recently published age from the same plutonic complex (Kröner et al., 2010). All ages are identical within analytical error; therefore, no additional information is yielded on the stages of batholith construction. Geochronology also confirms that the adjacent volcanic sequence is coeval with Gobi-Tianshan intrusive complex plutons.

Sm/Nd AND Rb/Sr ISOTOPE GEOCHEMISTRY

Thirty-four samples were selected to represent the range of compositions and paleodepths exposed in the Gobi-Tianshan intrusive complex. These samples include nine mafic dikes and mafic enclaves, nine granodiorites and andesites, and 16 granites and rhyolites.

Isotopic analyses were conducted at the University of Arizona according to procedures most recently described in Otamendi et al. (2009). The isotopic ratios of $^{87}Sr/^{86}Sr$, $^{143}Nd/^{144}Nd$, and the trace-element concentrations of Rb, Sr, Sm, and Nd were measured by thermal ionization mass spectrometry on whole-rock samples. Samples were spiked with the Caltech Rb, Sr, and mixed Sm-Nd spikes (Wasserburg et al., 1981; Ducea and Saleeby, 1998).

Mass spectrometric analyses were carried out at the University of Arizona on an automated VG Sector multicollector instrument fitted with adjustable 10^{11} Ω Faraday collectors and a Daly photomultiplier (Ducea and Saleeby, 1998). Concentrations of Rb, Sr, Sm, and Nd were determined by isotope dilution, with isotopic compositions determined on the same spiked runs. Runs consisted of acquisition of 100 isotopic ratios. Standards NRbAAA ($^{85}Rb/^{87}Rb$), Sr987 ($^{87}Sr/^{86}Sr$), nSmβ ($^{148}Sm/^{147}Sm$, $^{148}Sm/^{152}Sm$), and LaJolla Nd were utilized. The Sr isotopic ratios of standards and samples were normalized to $^{86}Sr/^{88}Sr = 0.1194$, and the Nd isotopic ratios were normalized to $^{146}Nd/^{144}Nd = 0.7219$. The 30 points presented for the Gobi-Tianshan intrusive complex in Figure 6 were age corrected to 292 Ma (Table 2). Procedural blanks averaged from five determinations were: Rb 10 pg, Sr 150 pg, Sm 2.7 pg, and Nd 5.5 pg.

Figure 6 shows Gobi-Tianshan intrusive complex data separated by bulk composition into mafic dikes and enclaves, granodiorites and andesites, and granites and rhyolites. All samples analyzed yielded positive $\varepsilon_{Nd(292)}$ values. Granites and granodiorites show a dominant grouping between $\varepsilon_{Nd(292)}$ +2 and +4, but range from 0 to +8 over a narrow $^{87}Sr/^{86}Sr_{(292)}$ range of 0.7045 and 0.7055. This trend is near-vertical in $^{87}Sr/^{86}Sr_{(292)}$ versus $\varepsilon_{Nd(292)}$, and significantly steeper than the mantle array. The upper portion of this trend is defined by abundant mafic enclaves in granodiorite units as well as late intruding mafic dikes. Several late granite sheets and rhyolitic volcanic samples display a striking

Geological Society of America Bulletin, published online on 2 October 2012 as doi:10.1130/B30324.1

TABLE 1. U-Pb RATIOS FOR GEOCHRONOLOGICAL ANALYSES

	Weighted avg.			% err		% err	Corr	$^{206}Pb/^{238}U$ age	
	Age (Ma)	Error (2σ)	$^{207}Pb^*/^{235}U$	(1σ)	$^{206}Pb^*/^{238}U$	(1σ)	coeff.	Age (Ma)	Error (2σ)
Sample 15407: 4783087°N, 384726°E									
15407-1	292	13	0.3853	6.85	0.05086	6.569	0.9412	319.8	20.49
15407-2			0.3341	7.967	0.04697	6.648	0.8453	295.9	19.23
15407-3			0.3149	10.16	0.04358	7.021	0.6822	275	18.9
15407-4			0.3814	18.54	0.04607	9.142	0.6544	290.4	25.96
15407-5			0.4082	10.91	0.04475	7.673	0.6063	282.2	21.19
15407-6			0.3764	8.736	0.04915	6.491	0.7963	309.3	19.6
15407-7			0.3592	15.4	0.04445	8.313	0.6158	280.3	22.8
15407-8			0.3243	10.81	0.04696	6.771	0.5683	295.8	19.58
15407-9			0.2887	12.52	0.04409	7.7	0.5275	278.1	20.96
15407-10			0.3359	14.75	0.0467	7.3	0.5835	294.3	21
Sample 5406: 4756806°N, 407082°E									
5406-1	290	12	0.335	10.51	0.04641	7.7	0.6938	292.5	22.01
5406-2			0.3446	10.86	0.04908	7.326	0.8055	308.9	22.09
5406-3			0.2349	19.35	0.04064	5.676	0.4078	256.8	14.29
5406-4			0.321	9.047	0.0467	6.845	0.7396	294.2	19.69
5406-5			0.3283	11.84	0.04737	6.807	0.666	298.4	19.85
5406-6			0.3475	11.27	0.0473	8.54	0.8605	297.9	24.86
5406-7			0.2563	12.69	0.0453	6.316	0.54	285.6	17.65
5406-8			0.3256	11.19	0.05125	7.603	0.6807	322.2	23.89
5406-9			0.3142	8.492	0.04391	6.081	0.7768	277	16.49
5406-10			0.316	11.73	0.04803	7.176	0.7507	302.4	21.2
5406-11			0.3361	8.312	0.04886	7.01	0.8229	307.5	21.05
Sample 1407, 4783602°N, 395123°E									
1407-1	293	6	0.3257	6.731	0.04609	5.256	0.8407	290.5	14.93
1407-2			0.3301	6.017	0.0462	4.264	0.7609	291.1	12.14
1407-3			0.3386	5.229	0.04587	4.121	0.7879	289.1	11.65
1407-4			0.3106	5.574	0.04394	4.053	0.7855	277.2	11
1407-5			0.3302	5.252	0.0457	3.775	0.7255	288.1	10.63
1407-6			0.3371	4.269	0.04646	3.952	0.932	292.8	11.31
1407-7			0.3139	5.927	0.04603	4.028	0.6193	290.1	11.43
1407-8			0.3394	5.007	0.04779	4.327	0.8183	301	12.72
1407-9			0.3266	6.157	0.04592	3.883	0.6871	289.4	10.99
1407-10			0.3373	4.638	0.04759	4.128	0.8417	299.7	12.09
1407-11			0.3408	6.437	0.04841	4.133	0.5018	304.8	12.3
1407-12			0.3653	4.793	0.04806	3.926	0.868	302.6	11.6
1407-13			0.3504	5.5	0.04827	4.024	0.737	303.9	11.94
1407-14			0.2967	6.314	0.04635	4.26	0.5912	292.1	12.16
1407-15			0.3393	4.894	0.04501	4.101	0.7682	283.8	11.39
Sample 12207: 4777175°N, 372738°E									
12207-1	295	7	0.3323	7.504	0.04779	3.919	0.5432	300.9	11.52
12207-2			0.3411	3.603	0.0477	2.97	0.9376	300.4	8.715
12207-3			0.3235	6.882	0.04643	3.493	0.6079	292.5	9.991
12207-4			0.5216	12.28	0.07093	4.214	0.4876	~~441.8~~	~~17.99~~
12207-5			0.2763	16.33	0.04557	4.453	0.5012	287.3	12.51
12207-6			0.3194	4.38	0.04614	2.779	0.7302	290.8	7.902
12207-7			0.2995	7.934	0.03993	4.731	0.6565	~~252.4~~	~~11.71~~
12207-8			0.3227	5.284	0.04643	3.409	0.7687	292.6	9.752
12207-9			0.297	8.126	0.04692	4.211	0.6418	295.6	12.16
12207-10			0.3264	4.102	0.04588	3.138	0.8596	289.2	8.873
12207-11			0.3239	6.465	0.04808	3.105	0.4431	302.7	9.182
12207-12			0.3465	3.617	0.04966	3.462	0.8187	312.4	10.56
12207-13			0.3762	8.774	0.04823	3.194	0.483	303.7	9.474
12207-14			0.3465	4.792	0.04955	3.052	0.78	311.7	9.288
12207-15			0.303	3.592	0.04267	3.027	0.7638	269.3	7.984
12207-16			0.3457	5.935	0.0468	3.733	0.8124	294.9	10.76

Note: All grains were used in calculation of weighted mean ages excepting two grains in sample 12207, which were statistical age outliers.

trend toward evolved $^{87}Sr/^{86}Sr_{(292)}$ compositions, up to 0.711 (Fig. 5).

These distinctive trends are comparable with broader regional isotopic characteristics, as shown in Figures 6A–6G. Data are organized into two groups according to age, 400–320 Ma in gray symbols, and 310–270 Ma in black symbols. Devonian to Mississippian data collectively display a vertical $\varepsilon_{Nd(t)}$ trend similar to that seen in the Gobi-Tianshan intrusive complex (e.g., Alataw, Bogda, and S. Tu Ha data). Late Carboniferous to Permian data, where available, display trends toward enrichment in radiogenic Sr, also similar to that observed in the Gobi-Tianshan intrusive complex.

DISCUSSION

Regional Correlations

The dissected and telescoped nature of the Tianshan belt presents a significant challenge to unraveling the original geometry of the accretionary system. We aim to understand the predissection geometry based on comparison of geological characteristics of individual tectonic lenses in order to assess the implications of Gobi-Tianshan intrusive complex data to the broader Tianshan. Granites and plutons from the Gobi-Tianshan intrusive complex and those along strike in the Harlik belt are both high-K, felsic, vary from volcanic-arc granites to within-plate granites on geochemical discriminatory diagrams, and have identical evolved isotopic characteristics including $^{87}Sr/^{86}Sr_{(292)}$ up to 0.7152. Ages of plutons from the Harlik belt

Geological Society of America Bulletin, published online on 2 October 2012 as doi:10.1130/B30324.1

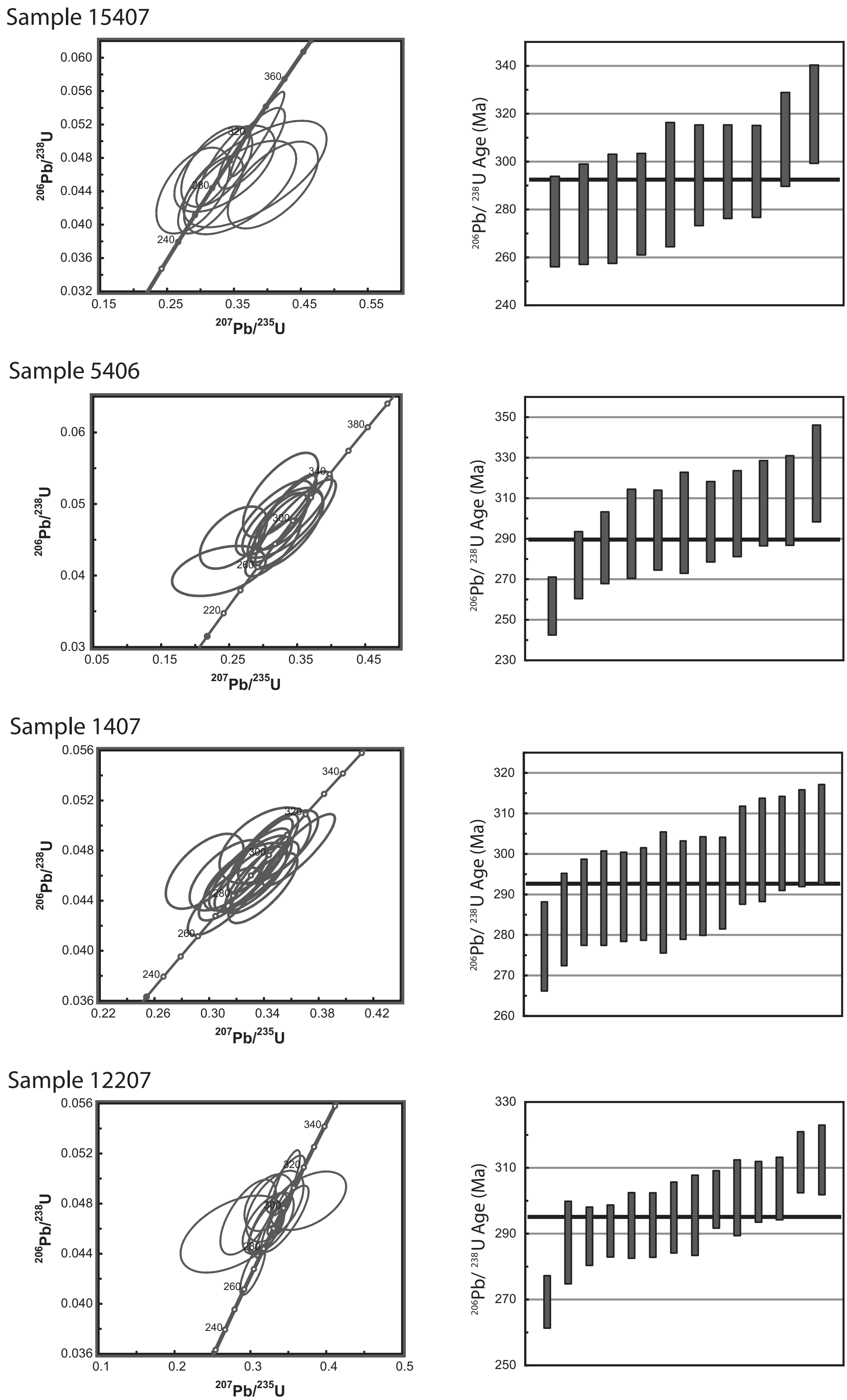

Figure 5. U-Pb concordia and weighted averages of four geochronology samples.

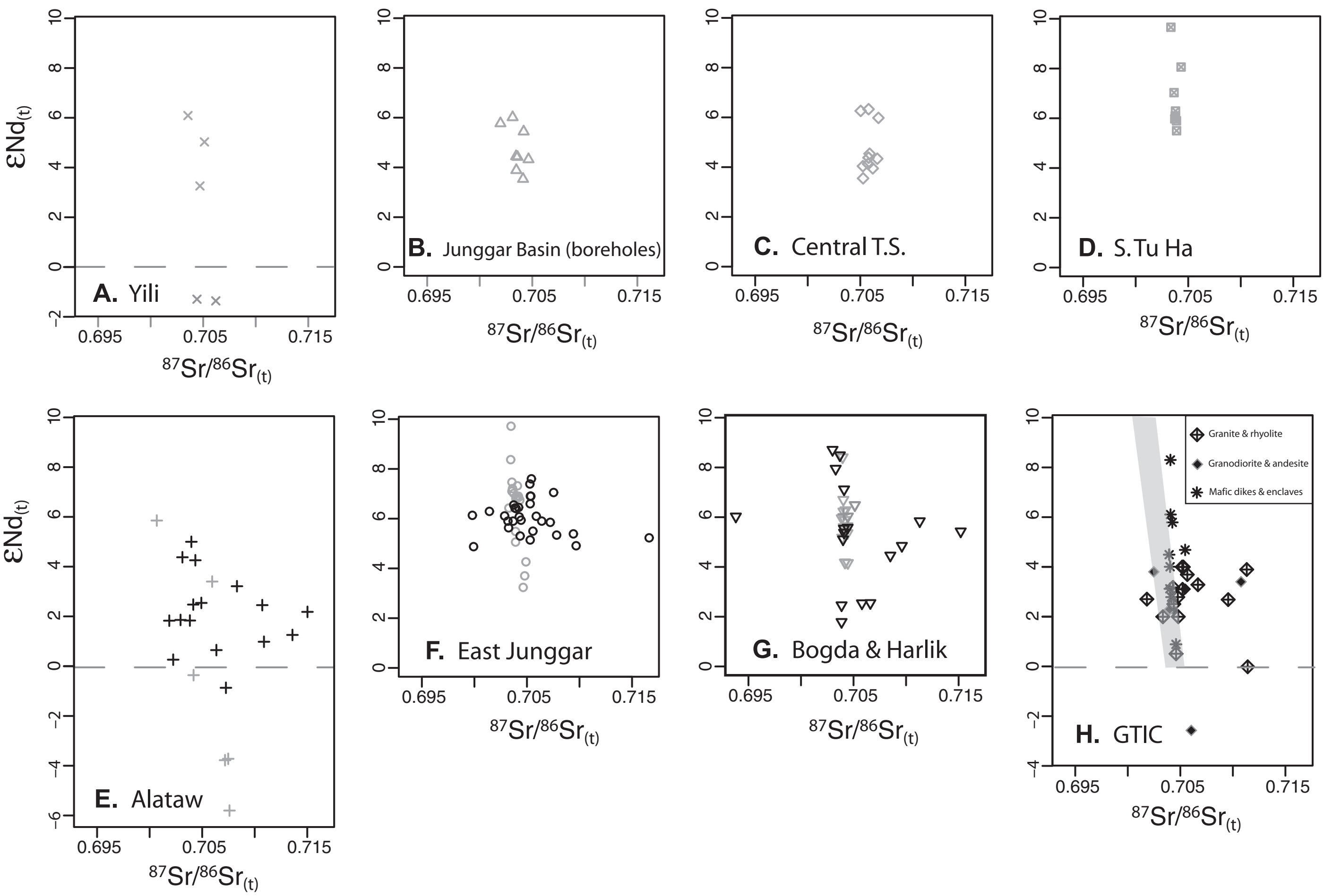

Figure 6. Age-corrected Sr and Nd isotopes from Tianshan granitoids and new data from the Gobi-Tianshan intrusive complex (GTIC). Black symbols—mid-Carboniferous; gray symbols—late Carboniferous–early Permian; gray field—calculated mantle array at 300 Ma. Data are from: Han et al. (1997); Chen et al. (2000); Chen and Jahn (2004); Xia et al. (2004); Zheng et al. (2007); Xia et al. (2008); Zhang et al. (2009b); and Tang et al. (2010). T.S.—Tianshan.

range from 288 Ma to 284 Ma (Yuan et al., 2010; Wang et al., 2010). To the north, the Harlik belt is bounded by the Kelameili fault zone (Charvet et al., 2007). We propose that this structure extends to the north of the Gobi-Tianshan intrusive complex, based primarily on the presence of undated mafic complexes northeast of the Gobi-Tianshan intrusive complex (Geomin, 2003; Hanzl et al., 2008b) and ophiolitic fragments to the east (Rippington et al., 2008) that may form a belt similar to that observed along the Kelameili fault zone (Xiao et al., 2009). Based on the timing and composition of granitic rocks and location of the bounding fault system, we interpret the Gobi-Tianshan intrusive complex to be structurally contiguous with the Harlik belt. This suggests that the Gobi-Tianshan intrusive complex is part of an E-W–oriented chain of large igneous bodies, possibly indicative of a magmatic arc. It has been argued that the Harlik belt (and by our correlation, the Gobi-Tianshan intrusive complex also) is contiguous with the East Junggar and therefore is part of a more northerly system that includes the Altay range, separate from the greater Tianshan (Charvet et al., 2007). However, the critical features linking these regions, Late Devonian to early Carboniferous volcaniclastic deposits, are more widespread than previously thought, as these were found in drill cores from the Junggar Basin (Zheng et al., 2007). Also, a common dike swarm between the Gobi-Tianshan intrusive complex and the Bogda region strengthens the correlation between the Gobi-Tianshan intrusive complex–Harlik range and the broader Tianshan (Figs. 1 and 2) (Allen et al., 1991; Shu et al., 2011). Regardless, based on the geochemistry presented here, we argue that all of these, Tianshan lenses, the Bogda Mountains, the East Junggar region, and the Gobi-Tianshan intrusive complex, experienced a similar Permian magmatic event and therefore may have been spatially related at that time.

Regional Magmatic Geochemical Characteristics

The Gobi-Tianshan intrusive complex displays first-order magmatic characteristics that corroborate a model of formation in a continental margin or fringing-arc setting. Granodioritic units, which make up >50% of the Gobi-Tianshan intrusive complex, ubiquitously contain hornblende and hornblende cumulates. The Gobi-Tianshan intrusive complex is a batholith-sized system, with ~3400 km^2 of exposed intrusive and extrusive material. If correlations with undated plutons ~40 km to the west are confirmed, the areal extent of the magmatic system could be significantly larger. Field and petrologic observations indicate that this system was a voluminous, intermediate, hydrated magma system of the kind most commonly formed during continental margin subduction. These characteristics make the Gobi-Tianshan

Geological Society of America Bulletin, published online on 2 October 2012 as doi:10.1130/B30324.1

TABLE 2. LOCATIONS IN UNIVERSAL TRANSVERSE MERCADOR (ZONE 47T, SPHEREOID WGS84) AND AGE-CORRECTED Rb-Sr AND Sm-Nd ISOTOPIC ANALYSES FROM THE GOBI-TIANSHAN INTRUSIVE COMPLEX

Rock type	Sample	Northing	Easting	Rb	Sr	Rb/Sr	$^{87}Rb/^{86}Sr$	$^{87}Sr/^{86}Sr$ (0)	Std err (%)	$^{87}Sr/^{86}Sr$ (292)
Basalt dike	1406	4788800	391947	38.919	496.618	0.0784	0.225289	0.704836	0.0011	0.703900
Rhyolite	5306	4757500	403802	134.379	63.473	2.1171	6.101423	0.730557	0.001	0.705206
Granite	5406	4756806	407082	87.5162	407.1689	0.214938	0.618016	0.706904	0.001	0.704336
Granite	6406B	4768260	390934	2191.525	25.5832	85.6628	248.6889	1.735121	0.0017	0.701817
Granite	12206B	4783450	395187	73.926	218.048	0.3381	0.972394	0.708279	0.0009	0.704239
Granodiorite	12406	4786957	395723	63.346	221.147	0.2864	0.823536	0.705921	0.0011	0.702499
Granodiorite	1407A	4783602	395123	89.8106	75.0146	1.197241	3.446966	0.720305	0.0012	0.705983
Enclave	1607A	4783901	394895	50.9215	403.0082	0.126354	0.363256	0.705471	0.0012	0.703962
Enclave	1607B	4783901	394895	41.6391	514.9433	0.080861	0.232459	0.704979	0.0014	0.704013
Granite	2707	4784462	395079	22.0423	134.9716	0.163311	0.469778	0.711411	0.0016	0.709459
Granodiorite	3207A	4785857	395523	54.2593	415.8698	0.130472	0.375104	0.705699	0.0011	0.704140
Enclave	3207B	4785857	395523	24.9748	480.0371	0.052027	0.149561	0.704675	0.001	0.704054
Andesite tuff	5407c	4762844	385268	17.0477	117.404	0.145205	0.417737	0.712405	0.001	0.710669
Enclave	6607	4764267	400994	23.65	567.65	0.041679	0.11983	0.705934	0.0012	0.705436
Porphyritic granite	6907	4765023	401340	27.0131	164.549	0.164164	0.472317	0.713245	0.0012	0.711283
Syenogranite	10907	4763456	403915	145.2629	52.5155	2.766097	7.97643	0.736482	0.0014	0.703340
Andesite dike	12207	4777175	372738	11.1704	328.7746	0.033977	0.097673	0.704637	0.0015	0.704231
Leucogranite	14907c	4787920	391049	6.5049	461.382	0.014099	0.04053	0.706764	0.0012	0.706596
Syenite	15407	4783087	384726	105.921	37.247	2.8437	8.218293	0.739366	0.0012	0.705219
Gabbro	17807	4783983	391471	1.18869	173.563	0.00685	0.019688	0.704095	0.0021	0.704013
Quartz diorite	33307	4787682	365263	13.819	432.7144	0.031937	0.091817	0.705647	0.001	0.705265
Quartz diorite	33607A	4788024	365562	37.9175	638.3188	0.059402	0.170763	0.70468	0.001	0.703970
Granodiorite	2508	4766112	409443	119.344	246.382	0.484385	1.393329	0.711057	0.0015	0.705268
Syenogranite	3808	4765120	409263	136.707	26.6332	5.132934	14.85416	0.772925	0.0011	0.711206
Rhyolite	5008	4761496	405410	143.897	152.401	0.944202	2.717542	0.716917	0.0018	0.705626
Granodiorite	5108	4761149	405536	56.936	370.066	0.153853	0.442338	0.706016	0.0012	0.704178
Rhyolite	5208I	4761464	405004	90.699	298.612	0.303735	0.873493	0.708737	0.001	0.705108
Basaltic andesite	8408C	4758981	411487	27.925	809.1085	0.034513	0.099217	0.704968	0.0009	0.704556
Basalt dike	8808A	4782463	374061	21.394	382.481	0.055936	0.160801	0.704818	0.001	0.704150
Hybrid granite	8808B	4782463	374061	35.602	186.059	0.191347	0.550191	0.70703	0.001	0.704744
Granite	8808C	4782463	374061	91.951	208.041	0.441988	1.271224	0.709858	0.0012	0.704576
Granite	9808A	4781830	374931	95.64	268.619	0.356042	1.023948	0.709029	0.0009	0.704774
Hybrid granite	9808B	4781830	374931	82.408	316.141	0.260669	0.749571	0.707765	0.0011	0.704651
Quartz diorite	12508A	4788303	364085	38.124	469.792	0.081151	0.2333	0.705334	0.001	0.704365

Rock type	Sample	Sm	Nd	Sm/Nd	$^{147}Sm/^{144}Nd$	$^{143}Nd/^{144}Nd$ (0)	Std err (%)	$^{143}Nd/^{144}Nd$ (292)	$\varepsilon_{Nd(292)}$
Basalt dike	1406	4.524	22.079	0.204899	0.123879	0.512731	0.0007	0.512494	4.5
Rhyolite	5306	4.784	24.131	0.198261	0.119863	0.512652	0.0008	0.512423	3.1
Granite	5406	5.1382	25.0489	0.205127	0.124013	0.512628	0.001	0.512391	2.5
Granite	6406B	1.8709	10.8619	0.172243	0.104132	0.512597	0.0011	0.512398	2.7
Granite	12206B	0.294	2.031	0.144988	0.087654	0.512593	0.0011	0.512425	3.2
Granodiorite	12406	4.166	21.358	0.195062	0.11793	0.512683	0.0011	0.512458	3.8
Granodiorite	1407A	8.291	40.5927	0.204249	0.123484	0.512372	0.0006	0.512136	–2.5
Enclave	1607A	5.5512	27.2318	0.203851	0.123243	0.512654	0.0012	0.512418	3.1
Enclave	1607B	6.0918	30.9532	0.196809	0.118986	0.512693	0.0012	0.512466	4.0
Granite	2707	0.695	4.0685	0.170937	0.103343	0.512596	0.0015	0.512398	2.7
Granodiorite	3207A	5.8353	28.2595	0.206491	0.124839	0.512652	0.0018	0.512413	3.0
Enclave	3207B					0.512689	0.0008	0.512689	8.3
Andesite tuff	5407c	3.34089	14.877	0.224563	0.135766	0.512695	0.0015	0.512435	3.4
Enclave	6607	5.989	29.03662	0.206287	0.124719	0.512742	0.0011	0.512504	4.7
Porphyritic granite	6907	4.7459	25.33112	0.187356	0.113266	0.512481	0.0009	0.512264	0.0
Syenogranite	10907	2.5873	11.1398	0.232259	0.140417	0.512632	0.0023	0.512364	2.0
Andesite dike	12207	1.959	8.39937	0.233264	0.141031	0.512831	0.0011	0.512561	5.8
Leucogranite	14907c	9.6835	43.9783	0.220188	0.133121	0.512685	0.0008	0.512431	3.3
Syenite	15407	7.669	40.522	0.189267	0.11426	0.512683	0.0009	0.512465	4.0
Gabbro	17807	1.443	4.7022	0.30686	0.185536	0.512928	0.001	0.512573	6.1
Quartz diorite	33307	5.552	28.778	0.192925	0.11672	0.512713	0.012	0.512490	4.4
Quartz diorite	33607A	5.9209	26.2861	0.225249	0.136179	0.512641	0.0009	0.512381	2.3
Granodiorite	2508	4.366	22.339	0.19546	0.118174	0.512648	0.0008	0.512422	3.1
Syenogranite	3808	5.888	26.29234	0.223956	0.1354	0.512723	0.0008	0.512464	3.9
Rhyolite	5008	8.949	41.953	0.2133	0.128964	0.512698	0.0008	0.512451	3.7
Granodiorite	5108	4.7494	20.5336	0.231304	0.139841	0.512678	0.001	0.512411	2.9
Rhyolite	5208I	6.554	30.389	0.21567	0.13048	0.512715	0.0011	0.512466	4.0
Basaltic andesite	8408C	4.9704	24.196	0.205425	0.12419	0.512546	0.0015	0.512309	0.9
Basalt dike	8808A	2.825	13.0494	0.216485	0.130973	0.512655	0.001	0.512405	2.8
Hybrid granite	8808B	3.299	21.007	0.157068	0.094958	0.512588	0.0011	0.512406	2.8
Granite	8808C	3.964	19.04	0.208181	0.125857	0.512526	0.0011	0.512285	0.5
Granite	9808A	4.149	21.216	0.19856	0.118233	0.512593	0.0009	0.512367	2.0
Hybrid granite	9808B	4.5918	21.0428	0.218213	0.131923	0.512570	0.001	0.512318	1.1
Quartz diorite	12508A	3.927	17.11927	0.22937	0.138672	0.512643	0.0011	0.512378	2.3

intrusive complex an unlikely candidate for a postamalgamation magmatic system, since generating such voluminous, intermediate magmatism with arc geochemical characteristics would require the remobilization of an unusually large amount of arc-modified lower crust (e.g., Yuan et al., 2010).

The Gobi-Tianshan intrusive complex is similar to Permian magmatic bodies in the Tianshan and East Junggar regions in several aspects. Intrusive bodies share a common magmatic style and chronology of voluminous granodioritic magmatism immediately followed by granite sheets or plutons (Chen et al., 2000; Chen and Jahn, 2004). Magmatism generated volumetrically significant units, some with general geochemical discriminators suggestive of an arc origin (Chen and Jahn, 2004; Yuan et al., 2010), although bodies to the far west trend toward significantly more alkaline compositions (Seltmann et al., 2010). Later bodies are also more alkaline in the Harlik belt (Wang et al., 2010) and in East Junggar (Han et al., 1997), similar to the magmatic chronology in the Gobi-Tianshan intrusive complex. The distinctive decoupling of Sr and Nd isotope variations is consistent across the region; $\varepsilon_{Nd(t)}$ varies from 0 to +8 with nearly invariant $^{87}Sr/^{86}Sr_{(t)}$ in Tianshan Carboniferous plutons. In latest Carboniferous to early Permian plutons, $^{87}Sr/^{86}Sr_{(t)}$ increases without a concurrent decrease in $\varepsilon_{Nd(t)}$ (Fig. 5). The result is a suite of rocks with highly elevated Sr isotope ratios suggestive of contamination by continental crust, but ubiquitously positive $\varepsilon_{Nd(t)}$ values generally indicative of primitive mantle sources. The coherence of this anomalous behavior in isotope ratios in Permian plutons across the Tianshan suggests that it is a signal of an orogenwide phenomenon and therefore provides a record of the geochemical consequences of first-order tectonic processes.

The observed isotope variations in Carboniferous plutons throughout the Tianshan and East Junggar generate a trend that is steeper than the mantle array. This trend therefore does not represent the more typical crustal covariation of Sr and Nd isotopes with time. In the Gobi-Tianshan intrusive complex, a potential depleted mantle source end member is recorded first in mafic enclaves in granodioritic plutons followed by crosscutting mafic dikes. The other end member is speculative but may represent ancient lower crust that was depleted in Rb in the deep past. This would imply that Proterozoic lower crust may be more widespread in the Tianshan than surface expression suggests (cf. Charvet et al., 2007).

It is notable that no significant shift in the range of $\varepsilon_{Nd(t)}$ compositions is observed between Carboniferous and Permian magmatism. Further, the mafic ε_{Nd} end member remained unchanged through the transition from calc-alkaline to alkaline magmatism. This invariant isotopic character of mafic inputs is an important first-order tectonic constraint. In a nonsubduction scenario, significant mantle heat input would be required to generate the increased volumes of magma that were emplaced during early Permian times. These models include hotspot magmatism as well as introduction of deeper mantle through delamination processes (e.g., Xia et al., 2004; Han et al., 2010). However, these models face the challenge of explaining how these processes occurred without a concurrent shift in mantle isotopic signatures.

The isotopic shift that occurs between the Carboniferous and the Permian is toward evolved radiogenic Sr isotopes without a concurrent shift in radiogenic Nd as observed in the Gobi-Tianshan intrusive complex, in the East Junggar, and in the Alataw area of the Yili block (Fig. 5). This trend has been explained by mixing of depleted mantle with a Proterozoic high-Sr crustal en member (Han et al., 1997; Chen et al., 2000). However, the regional consistency of this signal suggests that it represents an orogen-scale change in the crustal input into magmatic systems specific to the early Permian. Since the Tianshan crust was highly heterogeneous by Permian time, arguments based on regional-scale basement elemental and isotopic homogeneity are specious. Furthermore, it is uncertain why the additional integration of evolved continental material did not yield the more typical concave $^{87}Sr/^{86}Sr_{(t)}$ versus ε_{Nd} pattern, as is seen in Devonian plutons from the Chinese Altay (Yuan et al., 2007). We suggest that the simplest explanation for observed Sr isotope variations and the magmatic characteristics of early Permian magmatic systems is the interaction of isotopically evolved crustal sediments into Tianshan subduction zones (cf. Wang et al., 2009). Sediment influx could be due to shortening of distance between eroding land masses and subduction zones leading up to cessation of magmatism. Similar isotopic behavior is observed in calc-alkaline, medium- to high-K eruptions (e.g., Nila) in the Banda arc (Vroon et al., 1993). The underthrusting of sediments into the subduction zone, followed by increased traction due to a thickening downgoing plate explains (1) the transition in Sr isotopes, (2) the contemporaneous shift in tectonic stress and style of magmatism observed in the Gobi-Tianshan intrusive complex, and (3) the progression from typical hydrous intermediate arc magmatism to drier, more alkaline magmatism.

This model does not explicitly suggest an orientation of subduction, but the proximity of the Tarim margin to active magmatic systems is supported by the presence of volcanic sequences and mafic sills interlayered with early Permian Tarim margin sediments. Ages of these units range between 290 Ma and 260 Ma (Carroll et al., 1995). The interaction of cratonal sediments with at least one Tianshan subduction zone is corroborated by the presence of Proterozoic detrital zircons in a quartzofeldspathic schist metamorphosed at high pressure and low temperature in the South Tianshan accretionary complex/suture zone (Zhang et al., 2007).

Sedimentological evidence also suggests that the Carboniferous to early Permian was a time of significant tectonic transition. Upper Carboniferous sedimentary rocks along the Tarim margin, as well as in the southern Junggar Basin and northern Tu Ha Basin, are dominantly marine (Carroll et al., 1995, 2001), suggesting that the overall orogen topographic profile was low at this time. Basin closure across the entire region is suggested by a transition of sedimentary sequences from shallow marine to permanently regressive to subaerial from late Carboniferous to the middle Permian (Carroll et al., 1995). This shift was almost certainly diachronous; for example, a foredeep is proposed to have been active along the northwestern Tarim margin by early Permian time (Carroll et al., 2001), and contraction may have also occurred slightly earlier in the late Carboniferous to early Permian east of the Gobi-Tianshan intrusive complex in southern Mongolia (Lamb and Badarch, 2001; Johnson et al., 2008). This kind of deformation does not preclude ongoing subduction, as complex deformation (even concurrent contraction and extension) is well known in the end stages of basin closure such as in the Mediterranean region (Platt and Vissers, 1989). Additional geochronology in transitional sedimentary sections may help clarify the timing of uplift-related sedimentary variations between the Tianshan and southwestern Mongolia.

Mid-Permian amalgamation of the Tianshan is also consistent with ages of metamorphism and motion on faults throughout the Tianshan region. High-pressure metamorphism in the South Tianshan accretionary complex (Zhang et al., 2007), thrusting along major structures in the Chinese Altay (Briggs et al., 2009), and thrusting within the Tianshan (e.g., Yang et al., 2009) suggest a doubly vergent transpressional orogen in Permian–Triassic time. The earliest age for initiation of systemwide strike-slip faulting is commonly cited as 290–285 Ma, contemporaneous with the intrusion of the Gobi-Tianshan intrusive complex and other early Permian batholiths. However, only one region of the orogen, a section of mylonitized granites south of the Main Tianshan shear zone, consistently yields ages older than 275 Ma (Yin et al., 1998; Yin and Nye, 1996; Zhou et al., 2001; Laurent-Charvet et al., 2003), which are interpreted by many workers to be some combination of magmatic and metamorphic ages. All other $^{40}Ar/^{39}Ar$ ages fall in the range of 275–245 Ma, suggesting that major orogenwide wrench faulting postdated the intrusion of the Gobi-Tianshan intrusive complex by at least 5–10 m.y. (B. Wang et al., 2007; de Jong et al., 2009). All these results suggest the initiation of major metamorphism and strain-partitioned oblique convergence at ca. 285–280 Ma in southwest Mongolia, continuing through Permian–Triassic time (Xiao et al., 2009), consistent with the chronology of batholith emplacement, diking, and subsequent faulting observed in the Gobi-Tianshan intrusive complex.

In summary, the geological and petrological characteristics that suggest a volcanic-arc origin for the Gobi-Tianshan intrusive complex (Economos, 2009) are at odds with models of a pre-Permian amalgamation of this segment of the Tianshan. A subduction origin for early Permian magmatism does not require the remobilization of large volumes of arc-modified lower crust, which may be an unrealistic environment for a system of the size and composition of the Gobi-Tianshan intrusive complex. Isotopic characteristics provide a potential link between ca. 290 Ma granitoids across a large region of the Tianshan and East Junggar. Further, invariance of mantle components from the Carboniferous to Permian in these plutons must be explained by any formation model that suggests a dramatic mantle transition at this time, such as delamination or the initiation of a mantle plume. Anomalous elevated Sr isotope ratios are observed in early Permian plutons throughout the Tianshan; we suggest a possible explanation that this is the isotopic imprint of subducted continental sediments. This model may be corroborated by the presence of Proterozoic detrital grains in sedimentary rocks that underwent blueschist-facies metamorphism that are now found in the southern Tianshan, although these metamorphic rocks cannot be linked directly to the Gobi-Tianshan intrusive complex. Evidence from basin fill, ages of fault motion, and peak regional metamorphism throughout the mountain range is permissive of continued subduction at least in parts of Tianshan in earliest Permian time.

This study also improves our understanding of the structural link between late Paleozoic Tianshan compressional belts and suture zones studied in northeastern China (e.g., Li, 2006; Zhang et al., 2009; Hao, 2010). A structurally complex belt of Permian magmatism is observed across thousands of kilometers (e.g., Seltmann et al., 2010). The Gobi-Tianshan intrusive complex represents the easternmost well-documented continuation of this magmatic belt, and it points toward other potentially related intrusions in south-central Mongolia (Kovalenko et al., 2006; Rippington et al., 2008) and northeastern China (Zhang et al., 2009). The present study defines an age, magmatic style, and set of isotopic characteristics that may serve as markers for identifying related magmatism to the east in southern Mongolia, thus advocating the use of magmatic bodies as structural tracers in a zone where 250 m.y. of tectonic reactivation have disrupted more traditional structural correlations.

CONCLUSIONS

The 295–290 Ma Gobi-Tianshan intrusive complex shares structural, magmatic, isotopic, and age characteristics with Permian magmatic belts in the Tianshan and East Junggar, confirming the continuation of these belts into southern Mongolia. The Gobi-Tianshan intrusive complex is dominated by voluminous intermediate hydrated magmatism typical of a continental margin or continent-fringing arc. Complex isotope compositions reveal a consistent mantle signature for Carboniferous and early Permian plutons, but a dramatic shift in radiogenic Sr in a series of intrusive bodies across the central Tianshan, East Junggar, and southwestern Mongolia. We interpret this signature to represent the interaction of accretionary sediments with Tianshan subduction zone(s). At least in the eastern Tianshan, we argue that subduction continued but was waning in the early Permian, in contrast to models of a transtensional, poststructural amalgamation formation environment for ca. 290 Ma igneous intrusions. The Gobi-Tianshan intrusive complex represents a link east that allows for improved correlation with suture zones in eastern China, contributing to the goal of a complete model of the China-Mongolia portion of the world's largest accretionary orogen.

ACKNOWLEDGMENTS

This project was supported by a National Science Foundation International Doctoral Dissertation Enhancement Proposal OISE-0737907 and partially supported by the National Science Foundation Instrumentation and Facilities Program. The paper was improved by discussions with A.P. Barth and valuable reviews by A. Kröner, W.-j. Xiao, and D. Schofield. Special thanks go to Ochir Gerel, Adam Ianno, and Jennifer Leever.

REFERENCES CITED

Allen, M.B., Windley, B.F., Zhang, C., Zhao, Z.-Y., and Wang, G.-R., 1991, Basin evolution within and adjacent to the Tien Shan Range, NW China: Journal of the Geological Society of London, v. 148, p. 369–378, doi:10.1144/gsjgs.148.2.0369.

Badarch, G., Cunningham, D., and Windley, B., 2002, A new terrane subdivision for Mongolia: Implications for the Phanerozoic crustal growth of central Asia: Journal of Asian Earth Sciences, v. 21, p. 87–110, doi:10.1016/S1367-9120(02)00017-2.

Briggs, S.M., Yin, A., Manning, C.E., Zheng, L.-c., Wang, X.-f., and Grove, M., 2007, Late Paleozoic tectonic history of the Ertix fault in the Chinese Altai and its implications for the development of the Central Asian orogenic system: Geological Society of America Bulletin, v. 119, p. 944–960, doi:10.1130/B26044.1.

Briggs, S.M., Yin, A., Manning, C.E., Chen, Z.L., and Wang, X.F., 2009, Tectonic development of the southern Chinese Altai range as determined by structural geology, thermobarometry, $^{40}Ar/^{39}Ar$ thermochronology, and Th/Pb ion-microprobe monazite geochronology: Geological Society of America Bulletin, v. 121, p. 1381–1393, doi:10.1130/B26385.1.

Carroll, A.R., Graham, S.A., Hendrix, M.S., Ying, D., and Zhou, D., 1995, Late Paleozoic tectonic amalgamation of northwestern China: Sedimentary record of the northern Tarim, northwestern Turpan, and southern Junggar Basins: Geological Society of America Bulletin, v. 107, p. 571–594, doi:10.1130/0016-7606(1995)107<0571:LPTAON>2.3.CO;2.

Carroll, A.R., Graham, S.A., Chang, E.Z., and McKnight, C., 2001, Sinian through Permian tectonostratigraphic evolution of the northwestern Tarim basin, China, *in* Hendrix, M.S., and Davis, G.A., eds., Paleozoic and Mesozoic Tectonic Evolution of Central Asia: From Continental Assembly to Intracontinental Deformation: Geological Society of America Memoir 194, p. 47–69.

Charvet, J., Shu, L., and Laurent-Charvet, S., 2007, Paleozoic structural and geodynamic evolution of eastern Tianshan (NW China): Welding of the Tarim and Junggar plates: Episodes, v. 30, no. 3, p. 162–186.

Chen, B., and Jahn, B.M., 2004, Genesis of post-collisional granitoids and basement nature of the Junggar terrane, NW China: Nd-Sr isotope and trace element evidence: Journal of Asian Earth Sciences, v. 23, p. 691–703, doi:10.1016/S1367-9120(03)00118-4.

Chen, J., Zhou, T., Xie, Z., Zhang, X., and Guo, X., 2000, Formation of positive $\varepsilon_{Nd(T)}$ granitoids from the Alataw Mountains, Xinjiang, China, by mixing and fractional crystallization: Implication for Phanerozoic crustal growth: Tectonophysics, v. 328, p. 53–67, doi:10.1016/S0040-1951(00)00177-3.

Coleman, R.G., 1989, Continental growth of northwest China: Tectonics, v. 8, p. 621–635, doi:10.1029/TC008i003p00621.

Cunningham, W.D., Windley, B.F., Dorjnamjaa, D., Badamgarov, J., and Saandar, M., 1996, Late Cenozoic transpression in southwestern Mongolia and the Gobi–Altai–Tien Shan connection: Earth and Planetary Science Letters, v. 140, p. 67–81, doi:10.1016/0012-821X(96)00048-9.

de Jong, K., Wang, B., Faure, M., Shu, L., Cluzel, D., Charvet, J., Ruffet, G., and Chen, Y., 2009, New $^{40}Ar/^{39}Ar$ age constraint on the late Palaeozoic tectonic evolution of the western Tianshan (Xinjiang, northwestern China), with emphasis on Permian fluid ingress: International Journal of Earth Sciences, v. 98, p. 1239–1258, doi:10.1007/s00531-008-0338-8.

Dobretsov, N.L., Berzin, N., and Buslov, M., 1995, Opening and tectonic evolution of the paleo–Asian Ocean: International Geology Review, v. 37, p. 335–360, doi:10.1080/00206819509465407.

Ducea, M.N., and Saleeby, J.B., 1998, The age and origin of a thick mafic ultramafic root from beneath the Sierra Nevada batholith: Contributions to Mineralogy and Petrology, v. 133, p. 169–185, doi:10.1007/s004100050445.

Economos, R.C., 2009, Vertical Changes in Magmatic Architecture, Hybridization, and Geochemistry in a Tilted Arc Crustal Section of the Gobi-Tianshan Intrusive Complex, Mongolia [Ph.D. thesis]: Los Angeles, California, University of Southern California, 257 p.

Fillipova, I.B., Bush, V.A., and Didenko, A.N., 1990, Middle Paleozoic subduction belts: The leading factor in the formation of the Central Asian fold-and-thrust belt: Russian Journal of Earth Sciences, v. 4, no. 6, p. 405–426.

Gao, J., He, G., Li, M., Xiao, X., Yaoqing, T., Jun, W., and Zhao, M., 1995, The mineralogy, petrology, metamorphic PTDt trajectory and exhumation mechanism of blueschists, south Tianshan, northwestern China: Tectonophysics, v. 250, p. 151–168, doi:10.1016/0040-1951(95)00026-6.

Gao, J., Long, L., Klemd, R., Qian, Q., Liu, D., Xiong, X., Su, W., Liu, W., Wang, Y., and Yang, F., 2009, Tectonic evolution of the South Tianshan orogen and adjacent regions, NW China: Geochemical and age constraints of granitoid rocks: Journal of International Earth Sciences, v. 98, p. 1221–1238, doi:10.1007/s00531-008-0370-8.

Geomin, 2003, Geological and Geochemical Mapping of the Transaltai Gobi at a Scale of 1:200,000: Jihlava, Czech Republic, Geological Survey in Mongolia, official development assistance project of the Czech Republic, scale 1:200,000.

Gu, L.-x., Hu, S.-x., Yu, C.-s., Li, H.-y., Xiao, X.-j., and Yan, Z.-f., 2000, Carboniferous volcanites in the Bogra orogenic belt of eastern Tianshan: Their tectonic implications: Acta Petrolei Sinica, v. 16, no. 3, p. 305–316.

Gu, L-x, Hu, S-x., Chu, Q., Yu, C-s., and Xiao, X-j., 2005, Pre-collision granites and post-collision intrusive assemblage of the Kelameili-Harlik orogenic belt: Acta Geologica Sinica, v. 73, no. 3, p. 316–329.

Han, B.-f., Wang, S.-g., Jahn, B.-m., Hong, D.-w., Kagami, H., and Sun, Y.-l., 1997, Depleted mantle source for the Ulungur River A-type granites from North Xinjiang, China: Geochemistry and Nd-Sr isotopic evidence, and implications for Phanerozoic crustal growth: Chemical Geology, v. 138, p. 135–159, doi:10.1016/S0009-2541(97)00003-X.

Han, B.-f., Guo, Z.-j., Zhang, Z.-c., Zhang, L., Chen, J.-f., and Song, B., 2010, Age, geochemistry, and tectonic implications of a late Paleozoic stitching pluton in the North Tian Shan suture zone, western China: Geological Society of America Bulletin, v. 122, p. 627–640, doi:10.1130/B26491.1.

Hanzl, P., Bat-Ulzii, D., Rejchrt, M., Kosler, J., Bolormaa, K., and Hrdlickova, K., 2008a, Geology and geochemistry of the Palaeozoic plutonic bodies of the Trans-Altay Gobi, SW Mongolia: Implications for magmatic processes in an accreted volcanic arc system: Journal of Geosciences, v. 53, p. 201–234.

Hanzl, P., and Krejci, Z., eds., 2008b, Geological map of the Trans-Altay Gobi: Prague, Czech Geological Survey, scale 1:500,000, ISBN 978-7075-706-2.

Hao, B-w., 2010, Chronology, geochemistry and tectonic settings of the Hadamiao granodiorite on the northern margin of the North China platform: Acta Geologica Sinica (English Edition), v. 84, n. 6, p. 1500–1513.

Hu, A., Zhang, G., Zhang, Q., and Chen, Y., 1998, Constraints on the age of basement and crustal growth in Tianshan orogen by Nd isotopic composition: Science in China Series D, v. 41, no. 6, p. 648–657, doi:10.1007/BF02878748.

Jahn, B.-m., Wu, F., and Chen, B., 2000a, Massive granitoid generation in Central Asia: Nd isotope evidence and implications for continental growth in the Phanerozoic: Episodes, v. 23, p. 82–92.

Jahn, B.-m., Wu, F., and Chen, B., 2000b, Granitoids of the Central Asian orogenic belt and continental growth in the Phanerozoic: Transactions of the Royal Society of Edinburgh–Earth Sciences, v. 91, p. 181–193, doi:10.1017/S0263593300007367.

Johnson, C.L., Amory, J.A., Zinniker, D., Lamb, M.A., Graham, S.A., Affolter, M., and Badarch, G., 2008, Sedimentary response to arc-continent collision, Permian, southern Mongolia, *in* Draut, A.E., Clift, P.D., and Scholl, D.W., eds., Formation and Applications of the Sedimentary Record in Arc Collision Zones: Geological Society of America Special Paper 436, p. 363–390.

Kovalenko, V.I., Yarmoluyk, V.V., Sal'nikova, E.B., Kozlovsky, A.M., Kotov, A.B., Kovach, V.P., Savatenkov, V.M., Vladykin, N.V., and Ponomarchuk, V.A., 2006, Geology, geochemistry, and geodynamics of the Khan Bogd alkali granite pluton in southern Mongolia: Geotectonics, v. 40, no. 6, p. 450–466, doi:10.1134/S0016852106060033.

Kröner, A., Windley, B.F., Badarch, G., Tomurtogoo, O., Hegner, E., Jahn, B.M., Gruschka, S., Khain, E.V., Demoux, A., and Wingate, M.T.D., 2007, Accretionary growth and crust formation in the Central Asian orogenic belt and comparison with the Arabian-Nubian Shield, *in* Hatcher, R.D., Carlson, M.P., McBride, J.H., and Martínez Catalán, J.R., eds., 4-D Framework of Continental Crust: Geological Society of America Memoir 200, p. 181–209, doi: 10.1130/2007.1200(11).

Kröner, A., Lehmann, J., Schulmann, K., Demoux, A., Lexa, O., Tomurhuu, D., Štipská, P., Liu, D., and Wingate, M.T.D., 2010, Lithostratigraphic and geochronological constraints on the evolution of the Central Asian orogenic belt in SW Mongolia: Early Paleozoic rifting followed by late Paleozoic accretion: American Journal of Science, v. 310, p. 523–574, doi:10.2475/07.2010.01.

Lamb, M.A., and Badarch, G., 2001, Paleozoic sedimentary basins and volcanic arc systems of southern Mongolia: New geochemical and petrographic constraints, *in* Hendrix, M.S., and Davis, G.A., eds., Paleozoic and Mesozoic Tectonic Evolution of Central Asia: From Continental Assembly to Intracontinental Deformation: Geological Society of America Memoir 149, p. 117–149.

Laurent-Charvet, S., Charvet, J., Monié, P., and Shu, L.-s., 2003, Late Paleozoic strike-slip shear zones in eastern Central Asia (NW China): New structural and geochronological data: Tectonics, v. 22, 1009, doi:10.1029/2001TC901047.

Li, J-y., 2006, Permian geodynamic setting of Northeast China and adjacent regions: Closure of the Paleo-Asian Ocean and subduction of the Paleo-Pacific plate: Journal of Asian Earth Sciences, v. 26, p. 207–224.

Li, Y.-j., Li, Z.-c., Tong, L.-l., Gao, Z.-h., and Tong, L.-m., 2010, Revisit the constraints on the closure of the Tianshan ancient oceanic basin: New evidence from Yining block of the Carboniferous: Acta Petrolei Sinica, v. 26, no. 10, p. 2905–2912.

Long, L.-l., Gao, J., Wang, J.-b., Qian, Q., Xiong, X.-m., Wang, Y.-w., Wang, L.-j., and Gao, L.-m., 2008, Geochemistry and SHRIMP zircon U-Pb age of post-collisional granites in southwest Tianshan orogenic belt of China: Examples from the Heiyingshan and Laohutai plutons: Acta Geologica Sinica, v. 28, no. 2, p. 415–424.

Molnar, P., and Tapponnier, P., 1975, Cenozoic tectonics of Asia: Effects of a continental collision: Science, v. 189, no. 4201, p. 419–426, doi:10.1126/science.189.4201.419.

Otamendi, J.E., Ducea, M.N., Tibaldi, A.M., Bergantz, G.W., de la Rosa, J.D., and Vujovich, G.I., 2009, Generation of tonalitic and dioritic magmas by coupled partial melting of gabbroic and metasedimentary rocks within the deep crust of the Famatinian magmatic arc, Argentina: Journal of Petrology, v. 50, p. 841–873, doi:10.1093/petrology/egp022.

Paces, J.B., and Miller, J.D., 1993, Precise U-Pb ages of Duluth Complex and related mafic intrusions, northeastern Minnesota; geochronological insights to physical, petrogenetic, paleomagnetic, and tectonomagnetic processes associated with the 1.1 Ga Midcontinent Rift system: Journal of Geophysical Research, v. 98, p. 13,997–14,013, doi:10.1029/93JB01159.

Padilla, A.J., Economos, R.C., Anderson, J.L., and Paterson, S.R., 2008, Mafic-felsic magma interactions in an enclave megaplume, Gobi-Tianshan intrusive complex, southern Mongolia: Eos (Transactions, American Geophysical Union), v. 89, no. 53, Fall Meeting supplement, abstract V33A-2208.

Plafker, G., Nokleberg, W.J., and Lull, J.S., 1989, Bedrock geology and tectonic evolution of the Wrangellia, Peninsular, and Chugach terranes along the trans-Alaska crustal transect in the Chugach Mountains and southern Copper River basin, Alaska: Journal of Geophysical Research, v. 94, p. 4255–4295, doi:10.1029/JB094iB04p04255.

Platt, J.P., and Vissers, R.L.M., 1989, Extensional collapse of thickened continental lithosphere: A working hypothesis for the Alboran Sea and Gibraltar arc: Geology, v. 17, p. 540–543.

Rippington, S., Cunningham, D., and England, R., 2008, Structure and petrology of the Altan Uul ophiolite: New evidence for a late Carboniferous suture in the Gobi Altai, southern Mongolia: Journal of the Geological Society of London, v. 165, p. 711–723, doi:10.1144/0016-76492007-091.

Schmitt, A.K., Grove, M., Harrison, T.M., Lovera, O.M., Hulen, J., and Waters, M., 2003, The Geysers–Cobb Mountain magma system, California (Part 1): U-Pb zircon ages of volcanic rocks, conditions of zircon crystallization and magma residence times: Geochimica et Cosmochimica Acta, v. 67, p. 3423–3442, doi:10.1016/S0016-7037(03)00140-6.

Seltmann, R., Konopelko, D., Biske, G., Divaev, F., and Sergeev, S., 2010, Hercynian post-collisional magmatism in the context of Paleozoic magmatic evolution of the Tien Shan orogenic belt: Journal of Asian Earth Sciences, v. 42, p. 821–838.

Şengör, A.M.C., and Natal'in, B.A., 1996, Paleotectonics of Asia: Fragments of a synthesis, *in* Yin, A., and Harrison, M., eds., The Tectonic Evolution of Asia: Cambridge, UK, Cambridge University Press, p. 486–640.

Shu, L-s., Wang, B., Zhu, W-b., Guo, Z-j., Charvet, J., and Zhang, Y., 2011, Timing of initiation of extension in the Tianshan, based on structural, geochemican and geochronological analyses of bimodal volcanism and olistostrome in the Bogda Shan (NW China): International Journal of Earth Sciences, v. 100, p. 1647–1663.

Su, W., Gao, J., Klemd, R., Li, J.-l., Zhang, X., Li, X.-h., Chen, N.-s., and Zhang, L., 2010, U-Pb zircon geochronology of Tianshan eclogites in NW China: Implication for the collision between the Yili and Tarim blocks of the southwestern Altaids: European Journal of Mineralogy, v. 22, p. 473–478, doi:10.1127/0935-1221/2010/0022-2040.

Tang, G.-j., Wang, Q., Wyman, D.A., Sun, M., Li, Z.-x., Zhao, Z.-h., Sun, W.-d., Jia, X.-h., and Jiang, Z.-q., 2010, Geochronology and geochemistry of late Paleozoic magmatic rocks in the Lamasu-Dabate area, northwestern Tianshan (west China): Evidence for a tectonic transition from arc to post-collisional setting: Lithos, v. 119, p. 393–411, doi:10.1016/j.lithos.2010.07.010.

Vroon, P.Z., van Bergen, M.J., White, W.M., and Varekamp, J.C., 1993, Sr-Nd-Pb isotope systematics of the Banda arc, Indonesia: Combined subduction and assimilation of continental material: Journal of Geophysical Research, v. 98, p. 22,349–22,366, doi:10.1029/93JB01716.

Wang, B., Shu, L.-s., Faure, M., Cluzel, D., and Charvet, J., 2007, Paleozoic tectonism and magmatism of Kekesu-Qiongkushitai section in southwestern Chinese Tianshan and their constraints on the age of the orogeny: Acta Geologica Sinica, v. 23, no. 6, p. 1354–1368.

Wang, B., Faure, M., Shu, L., Cluzel, D., Charvet, J., de Jong, K., and Chen, Y., 2008, Paleozoic tectonic evolution of the Yili block, western Chinese Tianshan: Bulletin de la Société Géologique de France, v. 179, p. 483–490, doi:10.2113/gssgfbull.179.5.483.

Wang, B., Cluzel, D., Shu, L., Faure, M., Charvet, J., Chen, Y., Meffre, S., and de Jong, K., 2009, Evolution of calc-alkaline to alkaline magmatism through Carboniferous convergence to Permian transcurrent tectonics, western Chinese Tianshan: International Journal of Earth Sciences, v. 98, p. 1275–1298.

Wang, C.-s., Zhang, Z.-z., Gu, L.-x., Wu, C.-z., Tang, J.-h., Li, Z.-h., Feng, H., and Lei, R.-x., 2010, Zircon geochronology and geochemical characteristics of the Permian granitic complex at Yiwu, eastern Tianshan: Their tectonic significance: Acta Petrolei Sinica, v. 26, no. 4, p. 1045–1058.

Wang, Q., Wyman, D.A., Zhao, Z.-h., Xu, J.-f., Bai, Z.-h., Xiong, X.-l., Dai, T.-m., Li, C.-f., and Chu, Z.-y., 2007, Petrogenesis of Carboniferous adakites and Nb-enriched arc basalts in the Alataw area, northern Tianshan Range (western China): Implications for Phanerozoic crustal growth in the Central Asia orogenic belt: Chemical Geology, v. 236, p. 42–64, doi:10.1016/j.chemgeo.2006.08.013.

Wasserburg, G.J., Jacobsen, S.B., DePaolo, D.J., McCulloch, M.T., and Wen, T., 1981, Precise determination of Sm/Nd ratios, Sm and Nd isotopic abundances in standard solutions: Geochimica et Cosmochimica Acta, v. 45, p. 2311–2323, doi:10.1016/0016-7037(81)90085-5.

Xia, L.-q., Xu, X.-y., Xia, Z.-c., Li, X.-m., Ma, Z.-p., and Wang, L.-s., 2004, Petrogenesis of Carboniferous rift-related volcanic rocks in the Tianshan, northwestern China: Geological Society of America Bulletin, v. 116, p. 419–433, doi:10.1130/B25243.1.

Xia, L.-q., Xia, Z.-c., Xu, X.-y., Li, X.-m., and Ma, Z.-p., 2008, Relative contributions of crust and mantle to the generation of Tianshan Carboniferous rift-related basic lavas, northwestern China: Journal of Asian

Earth Sciences, v. 31, p. 357–378, doi:10.1016/j.jseaes.2007.07.002.

Xiao, W-j., Zhang, L-c., Qin, K-z., Sun, S., Li, J-l., 2004, Paleozoic accretionary and collisional tectonics of the eastern Tianshan (China): Implications for the continental growth of central Asia: American Journal of Science, v. 304, p. 370–395.

Xiao, W.-j., Windley, B.F., Huang, B.-c., Han, C.-m., Yuan, C., Chen, H.-l., Sun, M., Sun, S., and Li, J.-l., 2009, End-Permian to mid-Triassic termination of the accretionary processes of the southern Altaids: Implications for the geodynamic evolution, Phanerozoic continental growth, and metallogeny of Central Asia: International Journal of Earth Sciences, v. 98, p. 1189–1217, doi:10.1007/s00531-008-0407-z.

Xiao, W.-j., Huang, B.-c., Han, C.-m., Sun, S., and Li, J.-l., 2010, A review of the western part of the Altaids: A key to understanding the architecture of accretionary orogens: Gondwana Research, v. 18, p. 253–273, doi:10.1016/j.gr.2010.01.007.

Yang, T.-n., Li, J.-y., Wang, Y., and Dang, Y.-x., 2009, Late early Permian (266 Ma) N-S compressional deformation of the Turfan basin, NW China: The cause of change in basin pattern: International Journal of Earth Sciences, v. 98, p. 1311–1324, doi:10.1007/s00531-008-0396-y.

Yin, A., and Nie, S., 1996, A Phanerozoic palinspastic reconstruction of China and its neighboring regions, *in* Yin, A., and Harrison, M., eds., The Tectonic Evolution of Asia: Cambridge, UK, Cambridge University Press, p. 442–485.

Yin, A., Nie, S., Craig, P., Harrison, T.M., Ryerson, F.J., Qian, X-l., Yang, G., 1998, Late Cenozoic tectonic evolution of the southern Chinese Tian Shan: Tectonics, v. 17, n. 1, p. 1-27.

Yuan, C., Sun, M., Xian, W.-j., Li, W.-h., Chen, H.-l., Lin, S.-f., Xia, X.-p., and Long, X.-p., 2007, Accretionary orogenesis of the Chinese Altai: Insights from Paleozoic granitoids: Chemical Geology, v. 242, p. 22–39, doi:10.1016/j.chemgeo.2007.02.013.

Yuan, C., Sun, M., Wilde, S., Xiao, W.-j., Xu, Y.-g., Long, X.-p., and Zhao, G.-c., 2010, Post-collisional plutons in the Balikun area, east Chinese Tianshan: Evolving magmatism in response to extension and slab breakoff: Lithos, v. 119, p. 269–288, doi:10.1016/j.lithos.2010.07.004.

Zhang, L.-F., Ai, Y.-L., Li, X.-P., Rubatto, D., Song, B., Williams, S., Song, S., Ellis, D., and Liou, J.-G., 2007, Triassic collision of western Tianshan orogenic belt, China: Evidence from a SHRIMP U-Pb dating of zircon from HP/UHP eclogitic rocks: Lithos, v. 96, p. 266–280, doi:10.1016/j.lithos.2006.09.012.

Zhang, Z., Mao, J., Du, A., Pirajno, F., Wang, Z., Chai, F., Zhang, Z., and Yang, J., 2008, Re-Os dating of two Cu-Ni sulfide deposits in northern Xinjiang, NW China, and its geological significance: Journal of Asian Earth Sciences, v. 32, p. 204–217, doi:10.1016/j.jseaes.2007.10.005.

Zhang, Z., Zhou, G., Kusky, T., Yan, S., Bailin, C., and Zhao, L., 2009, Late Paleozoic volcanic record of the Eastern Junggar terrane, Xinjiang, northwestern China: Major and trace element characteristics, Sr-Nd isotopic systematics and implications for tectonic evolution: Gondwana Research, v. 16, p. 201–215, doi:10.1016/j.gr.2009.03.004.

Zheng, J., Sun, M., Zhao, G., Robinson, P.T., and Wang, F., 2007, Elemental and Sr-Nd-Pb isotopic geochemistry of late Paleozoic volcanic rocks beneath the Junggar Basin, NW China: Implications for the formation and evolution of the basin basement: Journal of Asian Earth Sciences, v. 29, p. 778–794, doi:10.1016/j.jseaes.2006.05.004.

Zhou, D., Graham, S.A., Chang, E.Z., Wang, B., and Hacker, B., 2001, Paleozoic tectonic amalgamation of the Chinese Tian Shan: Evidence from a transect along the Dushanzi-Kuqa highway, *in* Hendrix, M.S., and Davis, G.A., eds., Paleozoic and Mesozoic Tectonic Evolution of Central Asia: From Continental Assembly to Intracontinental Deformation: Geological Society of America Memoir 149, p. 23–46.

Science Editor: Nancy Riggs
Associate Editor: David Ian Schofield

Manuscript Received 26 April 2010
Revised Manuscript Received 22 March 2012
Manuscript Accepted 16 April 2012

Printed in the USA